Larger spatial footprint of wintertime total precipitation extremes in a warmer climate

Emanuele Bevacqua[1], Ted Shepherd[2], Peter A. G. Watson[3], Sarah Sparrow[4], David C H Wallom[4], and Daniel M Mitchell[5]

[1]Department of Meteorology, University of Reading
[2]Reading University
[3]School of Geographical Sciences, University of Bristol
[4]University of Oxford
[5]University of Bristol

November 21, 2022

Abstract

The simultaneous occurrence of extremely wet winters at multiple locations in the same region can contribute to widespread flooding and associated socio-economic losses. However, the change in the spatial extent of precipitation extremes is largely overlooked in climate change assessments. Employing new multi-thousand-year climate model simulations, we show that under both 2.0°C and 1.5°C warming scenarios, wintertime precipitation extreme extents would increase over about 80-90% of the Northern Hemisphere. Stabilising at 1.5°C rather than 2°C would reduce the average magnitude of the increase by 1.6-2 times. According to the climate model, the increased extents are caused by increases in precipitation intensity increasing rather than changes in the spatial organisation of the events. Relatively small percentage increases in precipitation intensities (e.g., by 4%) can drive disproportionately larger, by 1-2 orders of magnitude, growth in the spatial extents (by 97%).

Larger spatial footprint of wintertime total precipitation extremes in a warmer climate

Emanuele Bevacqua[1], Theodore G. Shepherd[1], Peter A. G. Watson[2], Sarah Sparrow[3], David Wallom[3], and Dann Mitchell[2,4]

[1]Department of Meteorology, University of Reading, Reading, United Kingdom
[2]School of Geographical Sciences, University of Bristol, Bristol, United Kingdom
[3]Oxford e-Research Centre, Engineering Science, University of Oxford, Oxford, United Kingdom
[4]Cabot Institute for the Environment, University of Bristol, Bristol, United Kingdom

Key Points:

- The spatial extent of wintertime total precipitation extremes is projected to increase over most of the Northern Hemisphere in the future
- Changes in the spatial organisation, i.e. dependence, of precipitation extremes only marginally affect the spatial extents
- Increased precipitation extreme magnitudes can cause a disproportionate (even 20-90 times larger) increase in the precipitation extreme extents

Corresponding author: Emanuele Bevacqua, e.bevacqua@reading.ac.uk

Abstract

The simultaneous occurrence of extremely wet winters at multiple locations in the same region can contribute to widespread flooding and associated socio-economic losses. However, the change in the spatial extent of precipitation extremes is largely overlooked in climate change assessments. Employing new multi-thousand-year climate model simulations, we show that under both 2.0^{o}C and 1.5^{o}C warming scenarios, wintertime total precipitation extreme extents would increase over about 80-90% of the Northern Hemisphere. Stabilising at 1.5^{o}C rather than 2^{o}C would reduce the average magnitude of the increase by 1.6-2 times. According to the climate model, the increased extents are caused by increases in precipitation intensity increasing rather than changes in the spatial organisation of the events. Relatively small percentage increases in precipitation intensities (e.g., by 4%) can drive disproportionately larger, by 1-2 orders of magnitude, growth in the spatial extents (by 97%).

Plain Language Summary

One of the most impact-relevant and studied effects of global warming is the intensification of precipitation extremes. When extremely wet winters occur simultaneously at multiple locations within the same region, their cumulative impacts can be particularly high and enhanced as a result of limited resources available to cope with simultaneous damages. Despite the socio-economic effects of widespread extremes, climate change studies have typically disregarded the spatial extension of the extremes. Here, based on new multi-thousand-year climate model simulations, we show that - over most of the Northern Hemisphere - the spatial footprint of total wintertime precipitation extremes is projected to largely widen in the future. This widening results from a warmer, and therefore moister, atmosphere that will intensify precipitation. Holding global warming to 1.5^{o}C rather than 2^{o}C, in line with the Paris Agreement, would be beneficial to society as it could limit the increase in the extension by up to 2 times on average. To develop better preparedness for such extreme events, stakeholders should consider that a small increase in precipitation intensities (for example, by 4%) could result in large (by 100%) increases in spatial extent.

Keywords: Anthropogenic climate change, Future projections, Spatial statistics, Precipitation extremes, Compound events, Flooding hazard

1 Introduction

Extremely wet winters resulting from one or multiple precipitation events can contribute to flooding leading to severe socio-economic impacts. When such extremely wet conditions occur simultaneously at multiple locations within the same region, their impacts may be enhanced and lead to extreme cumulative losses (Leonard et al., 2014). In fact, widespread extreme events can affect the ability of governments and international (re-)insurance companies to respond to the emergency, given that resources and funds need to be provided at multiple locations and industrial sectors simultaneously (Enríquez et al., 2020; Kemter et al., 2020; Zscheischler et al., 2020). Recent extreme events showed that, as a result of persistent atmospheric conditions, extremely wet winters and associated flooding can affect multiple countries simultaneously and put high pressure on railway/road networks and transnational risk-reduction mechanisms (Jongman et al., 2014; Zscheischler et al., 2020). For example, the extremely wet winter of 2013/2014 in southern England, Wales, Ireland, and southern Norway led to major disruptions to transport and damages to livelihoods and infrastructure, and it was estimated to have caused hundreds of millions of pounds of insured losses (Kendon & McCarthy, 2015; Schaller et al., 2016).

Despite the relevance of the spatial extent of precipitation extremes for impacts, studies have focussed mainly on assessing the changes in the magnitude of the local precipitation extremes (Hoegh-Guldberg et al., 2018). In a future warmer climate, a moister atmosphere will favour higher precipitation magnitudes, while changes in the atmospheric circulation, e.g. storm track variations, may modulate both precipitation magnitudes and spatial patterns (e.g., Bevacqua et al., 2020c; O'Gorman & Schneider, 2009). As a result, these mechanisms may change the spatial extent of seasonal precipitation extremes. Recently, Berghuijs et al. (2019) found that the spatial extent of synchronous river flooding in Europe has increased during the last decades, although it was not demonstrated that anthropogenic climate change contributed to the increase (Kemter et al., 2020). To the best of our knowledge, the extent of wintertime total precipitation extreme events and its projected change under anthropogenic global warming has not yet been investigated.

Here, we close this research gap, focussing on precipitation in the Northern Hemisphere. A large sample size of data is required to analyse extremes of this type of *spatially compounding event* (Zscheischler et al., 2020), therefore we employ new multi-thousand-year climate model simulations.

2 Data and Methods

2.1 Data

We employ the citizen-science project climate*prediction*.net, which uses volunteers' personal computers, to simulate 1530 winters (December-February). We consider a present-day scenario (2006-2015; about 1^{o}C warmer than pre-industrial conditions in 1850-1900) and two future scenarios within which the world would be 1.5 and 2.0^{o}C warmer than pre-industrial conditions. We employ data from the global model of the atmosphere and land surface HadAM4 (Williams et al., 2003) with an increased resolution and a large ensemble (Watson et al., 2020; Bevacqua et al., 2020b). It considers 38 vertical levels and has a horizontal resolution of $\sim$60km at mid-latitudes ($0.83^o \times 0.56^o$ angular resolution), which is finer than that of many current global climate models and is sufficient for good simulation of extratropical synoptic features such as storms (Demory et al., 2014; Trzeciak et al., 2016; Watson et al., 2020). HadAM4 has a heritage to widely-used earlier models in the HadAM series and, being particularly memory-efficient, can be used to obtain multi-thousand-year ensembles through running on the volunteers' personal computers (Mitchell et al., 2017b). Following the HAPPI experiment design (see Mitchell et al. (2017a) for details), simulations of the three scenarios were driven by prescribed fields of sea surface temperature (SST), sea ice concentration (SIC), and atmospheric gas concentrations. The prescribed fields of the present-day scenario are time-dependent observations during 2006-2015. Simulations of the warmer scenarios were driven by prescribed SST and SIC fields obtained as the superposition of time-dependent observations and constant changes derived from CMIP5 multi-model means, while atmospheric gases are held at constant future values. The different realisation of the winter's weather was obtained via perturbing the initial conditions of each ensemble member on November 1st. For each scenario, we build an ensemble within which each of the ten yearly prescribed conditions during 2006-2015 is equally considered, i.e. our 1530 winters consist of 153 simulations of the 10 individual winters of 2006-2015. To assess the fidelity of the simulations for the purpose of the study we compare the results of the HadAM4 model with those obtained from ERA5 reanalysis (Hersbach et al., 2020).

2.2 Spatial scale extremes

We identify the occurrence of a local extreme event when the wintertime precipitation total is above the 10-year present-day return level ($T_{\mathrm{occur}} = 10$ year; Figure S1 in the supporting information). To characterize the spatial extent of seasonal precipitation extremes, we proceed similarly to Berghuijs et al. (2019) and Kemter et al. (2020), i.e. we consider the *spatial scale of synchronous wintertime precipitation extremes*, hereafter referred to as *spatial scale*. For a given winter and location of interest, the spatial scale is identified through recursively searching for the first circular area centred at the location (starting with a radius of 1km) within which less than half of the surface is affected by simultaneous extremes. *Spatial scale extremes* (SS) are defined as the 100-year return level of the spatial scale ($T_{\mathrm{SS}} = 100$ year).

Given the large sample size of the ensemble simulations, return levels are defined empirically (van der Wiel et al., 2019) (e.g, the 10-year return level is defined as the $(1-1/10)\cdot 100$th percentile). We test the sensitivity of the changes in the extreme spatial scale to the return periods employed, i.e. T_{occur} and T_{SS} (Tables S1-S5). We show results within the latitude band $(28,78)^o$N, however we consider data northward of 22^oS to robustly estimate spatial scales in the northernmost and southernmost locations.

2.3 Statistical significance

For any given location, the projected change is considered *statistically significant* if the future return level lies outside the present-day 95% confidence interval. We estimate such a confidence interval based on resampling of the interannual variability. That is, we build 1000 datasets through randomly resampling 1530 winters (153 per year) from the originally simulated present-day dataset. For each of the 1000 datasets, we compute the return level. The resulting 1000 return levels are then used to estimate the centred 95% confidence interval.

2.4 Drivers of the changes in spatial scale extremes

The multivariate probability density function (pdf) $f(P_1, ..., P_N)$ of the precipitation variables at all N locations can be decomposed into the product of the N marginal pdfs f_{P_i} of the precipitation at individual locations and the copula density c that describes the spatial dependencies in the precipitation field (Sklar, 1959). That is, $f(P_1, ..., P_N) = f_{P_1}(P_1) \cdot ... \cdot f_{P_N}(P_N) \cdot c(F_{P_i}(P_i), ..., F_{P_N}(P_N))$, where F_{P_i} is the cumulative distribution function (CDF) of P_i. Therefore, from a statistical perspective, the changes in the spatial scale extremes, which are associated with changes in $f(P_1, ..., P_N)$, can be decomposed into changes in (1) the magnitude of the precipitation extremes (i.e., from the marginal distributions) and (2) the spatial dependence between precipitation at neighbouring locations (i.e., the copula) (Bevacqua et al., 2020a).

We estimate (1) as $100 \cdot (SS_{\mathrm{magn}} - SS_{\mathrm{pres}})/SS_{\mathrm{pres}}$, where SS_{pres} is the extreme spatial scale in the present and SS_{magn} is the extreme spatial scale in a dataset that assumes changes in precipitation magnitude, but not in spatial dependence (pairwise Spearman's correlations and tail dependencies (Bevacqua et al., 2017)). Following Bevacqua et al. (2019) (and, e.g. Manning et al. (2019); Villalobos-Herrera et al. (2020)), this dataset is defined as $(F^{-1}_{P_{\mathrm{fut}\ 1}}(F_{P_{\mathrm{pres}\ 1}}(P_{\mathrm{pres}\ 1})), ..., F^{-1}_{P_{\mathrm{fut}\ \mathrm{N}}}(F_{P_{\mathrm{pres}\ \mathrm{N}}}(P_{\mathrm{pres}\ \mathrm{N}}))$, where $P_{\mathrm{pres}\ \mathrm{i}}$ and $F_{P_{\mathrm{pres}\ \mathrm{i}}}$ are the wintertime precipitation in the present and its empirical CDF, respectively; and $P_{\mathrm{fut}\ \mathrm{i}}$ and $F_{P_{\mathrm{fut}\ \mathrm{i}}}$ are the same, but for the future. Given that $F_{P_{\mathrm{pres}\ \mathrm{i}}}(P_{\mathrm{pres}\ \mathrm{i}})$ has a standard uniform distribution, the marginal pdfs of the variables in the dataset are as in the future; the copula is a function of the variables $(F_{P_{\mathrm{pres}\ 1}}(P_{\mathrm{pres}\ 1}), ..., F_{P_{\mathrm{pres}\ \mathrm{N}}}(P_{\mathrm{pres}\ \mathrm{N}}))$ and is, therefore, as in the present.

Similarly, we estimate (2) as $100 \cdot (SS_{\mathrm{dep}} - SS_{\mathrm{pres}})/SS_{pres}$, where SS_{dep} is the spatial scale's extreme in the dataset $(F^{-1}_{P_{\mathrm{pres}\ 1}}(F_{P_{\mathrm{fut}\ 1}}(P_{\mathrm{fut}\ 1})), ..., (F^{-1}_{P_{\mathrm{pres}\ \mathrm{N}}}(F_{P_{\mathrm{fut}\ \mathrm{N}}}(P_{\mathrm{fut}\ \mathrm{N}})))$, which assumes changes in precipitation spatial dependence (copula as in the future), but not in magnitude.

2.5 Area weighted aggregated statistics

All the statistics, such as median, pattern Spearman's correlations ($\rho^{pattern}_{\mathrm{Spearman}}$), and percentage of the analysed area, are weighted based on the grid-points' surfaces, using the R-packages *wCorr* (Emad & Bailey, 2017) and *spatstat* (Baddeley et al., 2004).

3 Results

3.1 Present-day spatial scale extremes

The present-day spatial scale extremes are shown in Figure 1. A small extreme spatial scale indicates that precipitation extremes tend to be localized, i.e. to not co-occur with extremes in the surrounding area. The hemispheric median of the spatial scale extremes is about $27{\cdot}10^5 km^2$ (i.e. a circular area associated with a radius of 930km), indicating that the considered events potentially extend across multiple countries. Note that, as local precipitation extreme magnitudes are defined based on local return levels, small and large extents are associated with small and large regional spatial dependencies in the precipitation field, respectively.

Across the Northern Hemisphere, there is large variability in the spatial scale extremes, hence in the spatial dependencies, of the precipitation field (Figure 1), which appears to be influenced by topography. In fact, there is a tendency towards larger and smaller spatial scale extremes at lower and higher altitudes, respectively (Figure S2), which is in line with the results found by Berghuijs et al. (2019) for European river flooding spatial scales. The largest spatial scale extremes occurs over northern Europe, Russian plains, eastern China, and oceans; i.e., typically over extended low altitude areas, where the occurrence of widespread precipitation extremes is not obstructed by the orography. For example, in Moscow (Russia), the most extended events are associated with an anomalous seasonal upper-level atmospheric jet over central Europe (Figure S3), which - given the flat topography - favours widespread precipitation extremes in the surrounding area. The mean altitude of the locations with the top 5% (1%) spatial scale extremes is 120m (70m), against an average altitude of 370m over the analysed area. In contrast, the lowest spatial scales are typically found across mountainous areas, where precipitation extremes can be localized due to orographic effects (Martius et al., 2016), such as the Rocky Mountains, Alps and Pyrenees, Scandinavian Mountains, Caucasus Mountains, Himalayas, and Gobi Desert. As a result, the mean altitude of the locations with the 5% (1%) smallest spatial scale extremes is 990m (1900m).

A comparison of the results based on the HadAM4 model and the ERA5 reanalysis is not possible for very extreme events due to the limited sample size of the reanalysis data (e.g., van den Hurk et al., 2015; van der Wiel et al., 2019). This is the case even when considering ERA5 data during the extended period 1980-2020, therefore we focus the evaluation on less extreme events. The biases in the wintertime mean and 5-year return level precipitation are in line with those of other global climate models (Figure S4a-f), with a good representation of broad-scale features (Flato et al., 2014; Watson et al., 2020). Even for the considered relatively low return levels (T_{occur} = 5 year, T_{SS} = 10 year), the spatial pattern of the spatial scale high values in ERA5 is spatially noisy compared to HadAM4 (Figure S4g-i), highlighting that large ensemble simulations are essential for analysing spatially extended wintertime precipitation extremes and that an evaluation of these events is challenging. Nevertheless, the similarity of the area-weighted spatial scale (median of the associated radius of 520km and 440km in HadAM4 and ERA5, respectively) and of the large-scale spatial pattern indicates that the HadAM4 model performs satisfactorily for the purpose of the study.

3.2 Projected changes in the spatial scale extremes and associated drivers

In a world 2^oC warmer than during pre-industrial conditions, the extent of precipitation extremes is projected to increase over 90% of the analysed area (Figure 2a; Figure S5a shows changes in km^2). Spatial scale extremes increase by 97% in median (note that the increase is higher on landmasses than over ocean). Notably, such an increase corresponds to a median growth of $29{\cdot}10^5 km^2$ in spatial scale, which is equal to more than 10 times the surface area of a country such as the United Kingdom. Over 20% of the analysed area, the spatial scale would increase by at least 250% ($72{\cdot}10^5 km^2$).

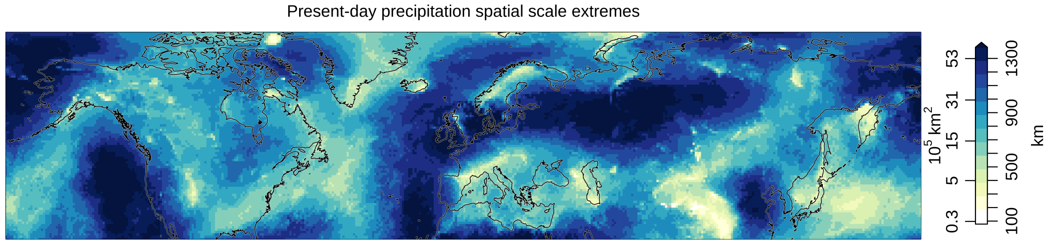

Figure 1. Present-day 100-year return level of the wintertime precipitation extremes' spatial scale (T_{occur} = 10 year; Methods). The colours indicate both the spatial scale value SS (i.e., a circular area in km^2) and the associated radius in km, i.e. $\sqrt{\text{SS}/\pi}$.

At the regional scale, the strongest percentage increase occurs over Canada, i.e 410% ($98{\cdot}10^5 km^2$; median over the box in Figure S5a). Over Northern Europe, a large increase in the spatial scale ($71{\cdot}10^5 km^2$; Figure S5a) combined with the relatively small present-day spatial-scale around the Scandinavian Mountains (Figure 1) results in a substantial, i.e. by 190%, increase in the extents. The increase is particularly large also over central and eastern Asia (260%; $62{\cdot}10^5 km^2$); however, note that the regional wintertime precipitation is frequently lower than about 18mm/winter (grey contours in Figure 2d), hence changes in the extremes' extents may have small impacts in this region. Overall, land areas with a substantial reduction in the extents are limited to Northern Africa, Spain and Portugal (-21%; $-7.1{\cdot}10^5 km^2$).

Most of the projected extent changes are incompatible with variations due to interannual variability (see stippling in Figure 2a), highlighting the presence of clear global warming induced effects. We move on to understanding the sources of these trends through decomposing the extent changes into the contributions from changes in the spatial dependence and magnitudes of the precipitation field.

3.2.1 Drivers of the changes in the spatial scale extremes

Changes in the spatial dependence of the precipitation field lead to generally small changes in the extent of the events (Figure 2b; median of about 0%). Such dependence-related changes are rarely statistically significant and do not exhibit a clear large-scale spatial pattern. The above indicates that the change in the spatial organisation of the wintertime precipitation extreme occurrences is generally unimportant for changes in the extreme spatial extents. Consistently, the changes in the spatial scales are dominated by the other potential driver, i.e. changes in the precipitation magnitude (compare Figure 2a and 2c; $\rho^{pattern}_{\text{Spearman}} = 0.94$). In fact, similarly to the actual changes in the spatial scale (Figure 2a), changes in the spatial scale resulting from precipitation magnitude changes (Figure 2c) are large, i.e. 93% in median, and positive over 92% of the analysed area. In line with this, the spatial pattern of the change in the precipitation extent resembles that of the change in the precipitation magnitudes (Figure 2a,d; $\rho^{pattern}_{\text{Spearman}} = 0.74$). Remarkably, relatively small regional percentage changes in precipitation magnitude can result in a large percentage change in the spatial extent of the extremes (Figure 2a,d). In fact, the median percentage increase in the spatial scale extremes (97%) is about 25 times larger than the increase in the magnitudes (4%).

From a physical perspective, all the above implies that the changes in the spatial extent can be solely understood in terms of the physical processes that modulate the changes in the precipitation extreme magnitudes. At the large scale, in line with other studies, precipitation magnitudes are projected to widely increase in percentage over the Northern Hemisphere landmasses, especially at high latitudes and over Asia, and to decrease around Northern Africa and northwestern Mexico (Figure 2d; Figure S5b shows changes in mm) (e.g., Knutti & Sedláček, 2013; Scoccimarro & Gualdi, 2020). The widespread increase in precipitation magnitudes arises from thermodynamic effects, i.e. in a warmer world, a higher atmospheric moisture holding capacity leads to more intense precipitation (e.g., Pfahl et al., 2017). However, atmospheric circulation changes, in which we have less confidence (Shepherd, 2014), will also substantially modulate regional precipitation changes and can either compensate or enhance the thermodynamic effect (Bevacqua et al., 2020c; Pfahl et al., 2017). To illustrate the different effects that documented atmospheric circulation changes can have on the magnitude, and therefore extent, of precipitation extremes, we now consider three case studies across the Northern Hemisphere.

To begin with, the strong reduction in precipitation magnitudes over northern Africa (about -10% in Marrakesh; Morocco) - which contributes to the reduced extents of the spatial scale extremes in the surrounding region - is in line with documented changes in the atmospheric circulation that would reduce both daily precipitation extremes (Pfahl et al., 2017) and total wintertime precipitation (Zappa & Shepherd, 2017). In Marrakesh, sustained upper-level winds over northern Africa - associated with enhanced storm track activity (Harvey et al., 2020; Zappa et al., 2015b) - favour high precipitation amounts around the city, northwestern Africa, and the eastern Mediterranean region (Figure 3a). In a warmer climate, this atmospheric circulation feature is expected to weaken (Figure 3b,c) in line with a documented weakening and reduction of storm intensity and frequency (Bevacqua et al., 2020c; Harvey et al., 2020; Pinto et al., 2007; Zappa et al., 2015a). As a result, precipitation extreme magnitudes and extents would decrease (Figure 3b), despite a higher atmospheric moisture content (Li et al., 2018; Pfahl et al., 2017).

Over the Scandinavian Peninsula, where extents are projected to increase strongly, precipitation magnitudes are projected to increase substantially, i.e. by about 10%, which is more than twice the hemispheric median increase. Wintertime precipitation extremes in this region are typically associated with an anomalously strong jet stream over the United Kingdom (Figure 3d). Under a 2^{o}C warming scenario, a strengthening and eastward extension of the jet stream over northern Europe would, therefore, favour the substantial increase in precipitation extremes and associated spatial extents (Figure 3e,f) (Harvey et al., 2020; Li et al., 2018; Zappa et al., 2013). Given that precipitation over the Scandinavian Peninsula is mainly driven by cyclones (Hawcroft et al., 2012; Pfahl & Wernli, 2012) and a sustained jet stream is associated with an increased cyclone activity, such an atmospheric circulation change would be consistent with a strengthening of the regional cyclonic activity (Harvey et al., 2020; Pinto et al., 2007; Zappa et al., 2013).

Finally, we consider the case of Wuhan (China), characterised by the highest projected increase in accumulated precipitation; the 10-year return level increases by more than 20% (about 90mm/winter). Around the Chinese city, precipitation extremes are associated with weakened upper-level winds across Japan and southern China (Figure 3g), in line with a weak East Asian winter monsoon (EAWM; L. Wang & Chen, 2014). The future strong intensification of precipitation is consistent with a general, i.e. on average and therefore during extreme events, weakening of the upper-level winds (Figure 3i,h). Such a wintertime evolution of the jet stream represents a plausible storyline of future atmospheric circulation change according to other climate model projections (Harvey et al., 2020; Li et al., 2018; Pinto et al., 2007), and appears in line with a projected weakening of the EAWM (Kitoh, 2006; H. Wang et al., 2013).

3.3 Difference between changes under 1.5^{o}C and 2.0^{o}C warming scenarios

Understanding how 0.5^{o}C less warming relative to +2.0^{o}C can reduce climate-related impacts is key for climate policies (Mitchell et al., 2016); gaining such an understanding requires large-ensemble simulations (Mitchell et al., 2017a). The general spatial pattern of the changes under 2.0^{o}C and 1.5^{o}C warming scenarios is similar ($\rho^{pattern}_{\mathrm{Spearman}} = 0.87$, increasing spatial scale extremes over 90% and 87% of the area, respectively; Figures 2a and S6a). However, the median increase in the spatial scale extremes would be about 1.6 times higher in a 2.0^{o}C (97%) than in a 1.5^{o}C warming scenario (60%). Such a difference is qualitatively

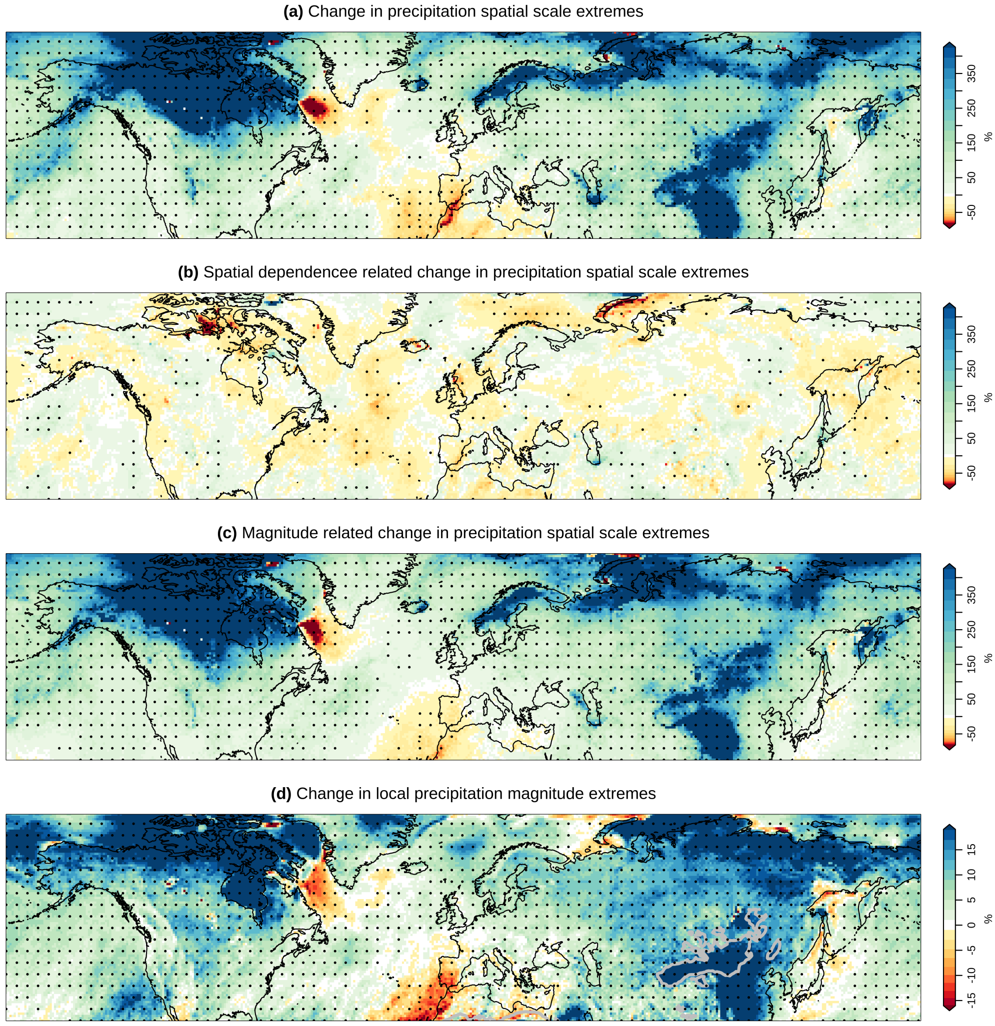

Figure 2. (a) Change in the 100-year return level of the wintertime precipitation extremes' spatial scale in a 2.0^{o}C warming scenario ($T_{\text{occur}} = 10$ year; Methods). Change in the spatial scale extremes caused by changes in (b) precipitation magnitudes and (c) spatial dependencies in the precipitation field. Stippling indicates statistically significant changes (Methods). (d) Change in the 10-year return level of the local wintertime precipitation total; grey contours over Asia enclose areas where the present-day 10-year return level is below 0.2mm/day (about 18mm/winter). The colour palette is chosen such that inverse changes between future and present values have the same colour intensity, e.g., -50% (halving) and +100% (doubling) are shown with the same colour intensity.

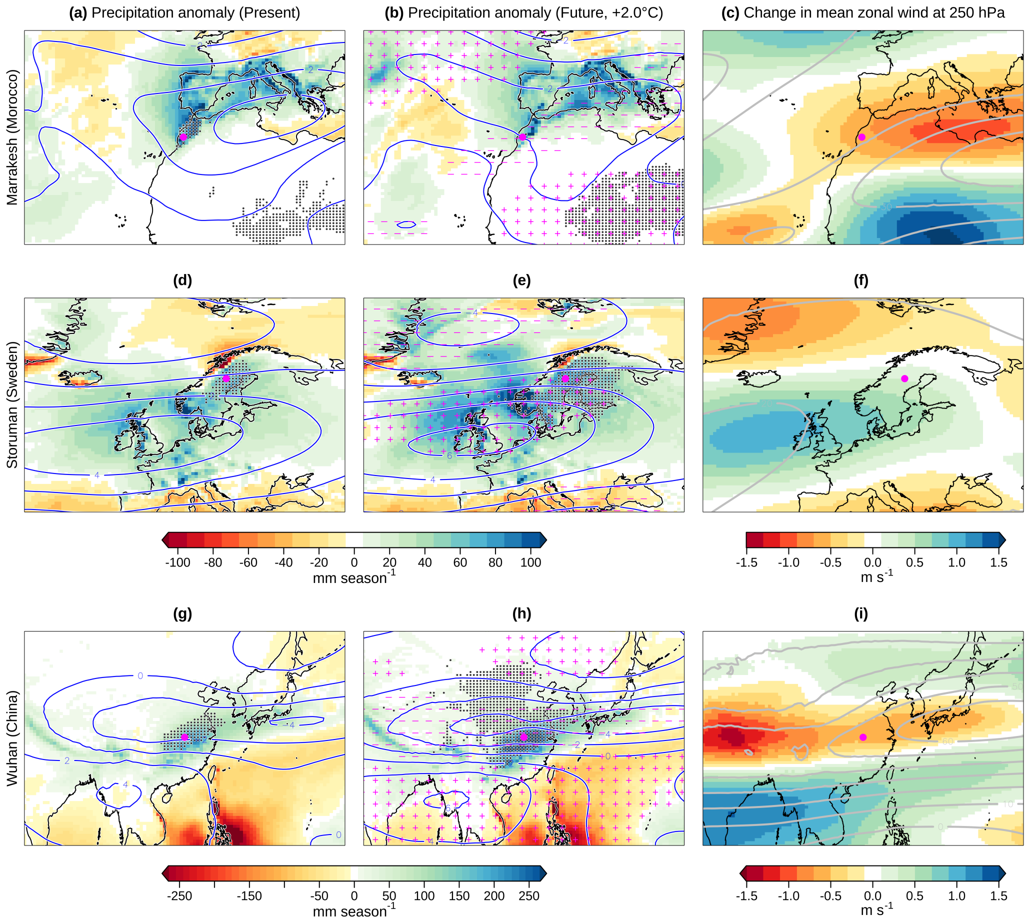

Figure 3. Average of the precipitation anomaly associated with extremely wet winters (> 10-year return level in present or future) in Marrakesh (Morocco; shown with a magenta dot) in (a) present climate and in (b) a $+2.0^{o}$C warming scenario. Contours show the average anomaly of the zonal wind at 250hPa in the extremely wet winters. Anomalies are relative to the present. Stippling indicates locations where the average precipitation is higher than the present-day 10-year return level. In (b), plus/minus signs indicate significantly positive/negative changes of the wind anomaly (i.e., future anomaly lying outside the present-day centred 95% confidence interval (CI); the CI is estimated through re-sampling present-day extreme events). (c) Shading shows the change in the average zonal wind at 250hPa (considering all winters) and contours show the average zonal wind in the present climate. Panels (d-f) and (g-i) are as in a-b, but for Storuman (Sweden) and Wuhan (China), respectively.

in line with the changes in precipitation magnitude, which increases by 4% and 3% in median under 2.0^{o}C and 1.5^{o}C warming scenarios, respectively (Figures 2d and S6b). Locally, i.e. over more than 32% (8%) of the area exposed to a larger extent in both scenarios compared to present, 0.5^{o}C more warming would lead to a doubling (quadrupling), at least, of the increase in the spatial scale extremes.

Parts of Spain and Portugal are the noticeable landmasses where the spatial scale extremes would increase in a 1.5^{o}C warming scenario, but reverse, i.e. decrease, in a 2.0^{o}C warming scenario (Figures S6a and 2a). Such a reversal is in line with the changes in precipitation intensities which would increase to a certain extent in a 1.5^{o}C scenario but decrease in a 2.0^{o}C scenario (Figures S6b and 2d). This is consistent with a strong weakening of the upper-level winds over northern Africa across the two scenarios (Figure S7), which would reverse the thermodynamically-driven precipitation increase (Li et al., 2018).

4 Discussion and Conclusions

The spatial extent of the wintertime total precipitation extremes is projected to increase notably across most of the Northern Hemisphere. Such growth in spatial extent is largely driven by increased wintertime precipitation extreme magnitudes. Given that extended high wintertime precipitation totals are driven by multiple weather systems moving across the same region (Hawcroft et al., 2012; Zappa et al., 2015a), our projection is consistent with the documented increase in the precipitation accumulated around the tracks of individual weather systems (Bevacqua et al., 2020c; Prein et al., 2017).

Our large-scale projection of precipitation extreme magnitudes, i.e. the main driver of the extent growth, is in line with projections from other modelling designs, including inter-comparsons, e.g. CMIP (Pfahl et al., 2017; Knutti & Sedláček, 2013). Regionally, i.e. around the Mediterranean basin and Mexico, the direction of the future changes is more uncertain across models (Bevacqua et al., 2020c; Pfahl et al., 2017; Shepherd, 2014). In fact, regional precipitation extent changes can depend on the model-dependent storyline of atmospheric circulation response to climate change (Bevacqua et al., 2020c; Zappa & Shepherd, 2017). Therefore, users interested in regional-scale changes in precipitation spatial extents should interpret our projection as a specific plausible storyline. For example, a weaker reduction of the upper-level winds over northern Africa than that found here is also plausible and could lead to a weaker decrease in the magnitude and spatial scales of precipitation extremes around southern Europe (Bevacqua et al., 2020c; Zappa, 2019; Zappa et al., 2015b). We find that changes in the spatial organisation, i.e. dependencies, of the precipitation extremes only marginally affect the future extent changes. This is consistent with the unchanged topography that would constrain potential changes in the spatial dependencies. However, given that atmospheric circulation changes may also modulate dependency changes, we cannot exclude the plausibility of an alternative storyline characterised by changes in the spatial dependencies.

While further studies based on large ensemble simulations from alternative climate model setups will allow for a comprehensive assessment of the regional extent changes, our results indicate that an important contribution from intensified precipitation towards a growth in the extents is likely a general feature of climate models in areas of the world where higher wintertime precipitation extremes are projected. Notably, to assume that percentage changes in precipitation intensities will drive similar percentage changes in the extent would be highly misleading. In fact, relatively small percentage increases in precipitation intensities can drive disproportionately larger, by 1-2 orders of magnitude (Tables S2 shows the sensitivity to the return periods), increases in the extent of the events. The estimated spatial extent increase depends on the degree of extremeness of the considered events (Table S1).

Precipitation is a relevant driver of spatially extended flooding (Jongman et al., 2014), hence the growth in the precipitation extreme extents could substantially impact areas across the Northern Hemisphere. Stabilising global warming at 1.5^{o}C rather than 2^{o}C, in line with the Paris Agreement, may substantially reduce impacts. Our study can contribute to understanding flooding changes, which also depend on, e.g., soil moisture, snowmelt, exposure, and vulnerability dynamics (Brunner et al., 2020; Jongman et al., 2014; Kemter et al., 2020). Overall, neglecting the spatial footprint of precipitation extreme events could lead to underestimating the population that is simultaneously affected by hazardous conditions. Hence, considering the effect of simultaneous extremes across neighbouring countries could allow for developing a better international preparedness for extreme events.

Acknowledgments

We acknowledge support from the NERC (DOCILE, NE/P002099/1). Peter Watson acknowledges the NERC IRF (NE/S014713/1). We thank JASMIN and CEDA for providing the facilities required to work with climate*prediction*.net. We thank the volunteers who have donated their computing time to climate*prediction*.net. We acknowledge William Ingram and Simon Wilson for their support in developing HadAM4 on CPDN. The data used in this study is available through Bevacqua et al. (2020b) at `http://doi.org/10.5281/zenodo.4311221`. ERA5 reanalysis is available through Hersbach et al. (2020) at `https://climate.copernicus.eu/climate-reanalysis`.

References

Baddeley, A. J., Turner, R., et al. (2004). *Spatstat: An R package for analyzing spatial point pattens.* University of Western Australia. Department of Mathematics and Statistics.

Berghuijs, W. R., Allen, S. T., Harrigan, S., & Kirchner, J. W. (2019). Growing spatial scales of synchronous river flooding in europe. *Geophysical Research Letters*, *46*(3), 1423–1428.

Bevacqua, E., Maraun, D., Hobæk Haff, I., Widmann, M., & Vrac, M. (2017). Multivariate statistical modelling of compound events via pair-copula constructions: analysis of floods in ravenna (italy). *Hydrology and Earth System Sciences*, *21*(6), 2701–2723.

Bevacqua, E., Maraun, D., Vousdoukas, M. I., Voukouvalas, E., Vrac, M., Mentaschi, L., & Widmann, M. (2019). Higher probability of compound flooding from precipitation and storm surge in europe under anthropogenic climate change. *Science advances*, *5*(9), 10.1126/sciadv.aaw5531. doi: 10.1126/sciadv.aaw5531

Bevacqua, E., Vousdoukas, M. I., Zappa, G., Hodges, K., Shepherd, T. G., Maraun, D., ... Feyen, L. (2020a). More meteorological events that drive compound coastal flooding are projected under climate change. *Communications earth & environment*, *1*(47). doi: 10.1038/s43247-020-00044-z

Bevacqua, E., Watson, P., Sparrow, S., & Wallom, D. (2020b). Multi-thousand-year simulations of december-february precipitation and zonal upper-level wind. *Zenodo*, *(Version 1.0.0) [Data set]*. Retrieved from `http://doi.org/10.5281/zenodo.4311221` doi: http://doi.org/10.5281/zenodo.4311221

Bevacqua, E., Zappa, G., & Shepherd, T. G. (2020c). Shorter cyclone clusters modulate changes in european wintertime precipitation extremes. *Environmental Research Letters*, *15*(124005). doi: 10.1088/1748-9326/abbde7

Brunner, M. I., Gilleland, E., Wood, A., Swain, D. L., & Clark, M. (2020). Spatial dependence of floods shaped by spatiotemporal variations in meteorological and land-surface processes. *Geophysical Research Letters*, *47*(13), e2020GL088000.

Demory, M.-E., Vidale, P. L., Roberts, M. J., Berrisford, P., Strachan, J., Schiemann, R., & Mizielinski, M. S. (2014). The role of horizontal resolution in simulating drivers of the global hydrological cycle. *Climate dynamics*, *42*(7-8), 2201–2225.

Emad, A., & Bailey, P. (2017). *wcorr: weighted correlations.–r package ver. 1.9. 1.*

Enríquez, A. R., Wahl, T., Marcos, M., & Haigh, I. D. (2020). Spatial footprints of storm surges along the global coastlines. *Journal of Geophysical Research: Oceans*, *125*(9), e2020JC016367.

Flato, G., Marotzke, J., Abiodun, B., Braconnot, P., Chou, S. C., Collins, W., ... others (2014). Evaluation of climate models. In *Climate change 2013: the physical science* *basis. contribution of working group i to the fifth assessment report of the intergovernmental panel on climate change* (pp. 741–866). Cambridge University Press.

Harvey, B., Cook, P., Shaffrey, L., & Schiemann, R. (2020). The response of the northern hemisphere storm tracks and jet streams to climate change in the CMIP3, CMIP5, and CMIP6 climate models. *Journal of Geophysical Research: Atmospheres*, e2020JD032701.

Hawcroft, M., Shaffrey, L., Hodges, K., & Dacre, H. (2012). How much northern hemisphere precipitation is associated with extratropical cyclones? *Geophysical Research Letters*, *39*(24).

Hersbach, H., Bell, B., Berrisford, P., Hirahara, S., Horányi, A., Muñoz-Sabater, J., ... others (2020). The era5 global reanalysis. *Quarterly Journal of the Royal Meteorological Society*, *146*(730), 1999–2049.

Hoegh-Guldberg, O., Jacob, D., Bindi, M., Brown, S., Camilloni, I., Diedhiou, A., ... others (2018). Impacts of 1.5^{o}C global warming on natural and human systems. *Global warming of 1.5^{o}C. An IPCC Special Report*.

Jongman, B., Hochrainer-Stigler, S., Feyen, L., Aerts, J. C., Mechler, R., Botzen, W. W., ... Ward, P. J. (2014). Increasing stress on disaster-risk finance due to large floods. *Nature Climate Change*, *4*(4), 264–268.

Kemter, M., Merz, B., Marwan, N., Vorogushyn, S., & Blöschl, G. (2020). Joint trends in flood magnitudes and spatial extents across europe. *Geophysical Research Letters*, *47*(7), e2020GL087464.

Kendon, M., & McCarthy, M. (2015). The uk's wet and stormy winter of 2013/2014. *Weather*, *70*(2), 40–47.

Kitoh, A. (2006). Asian monsoons in the future. In *The asian monsoon* (pp. 631–649). Springer.

Knutti, R., & Sedláček, J. (2013). Robustness and uncertainties in the new CMIP5 climate model projections. *Nature Climate Change*, *3*(4), 369–373.

Leonard, M., Westra, S., Phatak, A., Lambert, M., van den Hurk, B., McInnes, K., ... Stafford-Smith, M. (2014). A compound event framework for understanding extreme impacts. *Wiley Interdisciplinary Reviews: Climate Change*, *5*(1), 113–128.

Li, C., Michel, C., Graff, L. S., Bethke, I., Zappa, G., Bracegirdle, T. J., ... others (2018). Midlatitude atmospheric circulation responses under 1.5 and 2.0 degrees ^{o}C warming and implications for regional impacts. *Earth System Dynamics*, *9*(2), 359–382.

Manning, C., Widmann, M., Bevacqua, E., Van Loon, A. F., Maraun, D., & Vrac, M. (2019). Increased probability of compound long-duration dry and hot events in europe during summer (1950–2013). *Environmental Research Letters*, *14*(9), 094006.

Martius, O., Pfahl, S., & Chevalier, C. (2016). A global quantification of compound precipitation and wind extremes. *Geophysical Research Letters*, *43*(14), 7709–7717.

Mitchell, D., AchutaRao, K., Bethke, I., Beyerle, U., Ciavarella, A., Forster, P., ... others (2017a). Half a degree additional warming, prognosis and projected impacts (HAPPI): background and experimental design. *Geoscientific Model Development*, *10*, 571–583.

Mitchell, D., Davini, P., Harvey, B., Massey, N., Haustein, K., Woollings, T., ... others (2017b). Assessing mid-latitude dynamics in extreme event attribution systems. *Climate Dynamics*, *48*(11-12), 3889–3901.

Mitchell, D., James, R., Forster, P. M., Betts, R. A., Shiogama, H., & Allen, M. (2016). Realizing the impacts of a 1.5^{o}C warmer world. *Nature Climate Change*, *6*(8), 735–737.

O'Gorman, P. A., & Schneider, T. (2009). The physical basis for increases in precipitation extremes in simulations of 21st-century climate change. *Proceedings of the National Academy of Sciences*, *106*(35), 14773–14777.

Pfahl, S., O'Gorman, P., & Fischer, E. (2017). Understanding the regional pattern of projected future changes in extreme precipitation. *Nature Climate Change*, *7*(6), 423–427.

Pfahl, S., & Wernli, H. (2012). Quantifying the relevance of cyclones for precipitation extremes. *Journal of Climate*, *25*(19), 6770–6780.

Pinto, J. G., Ulbrich, U., Leckebusch, G., Spangehl, T., Reyers, M., & Zacharias, S. (2007). Changes in storm track and cyclone activity in three sres ensemble experiments with the echam5/mpi-om1 gcm. *Climate Dynamics*, *29*(2-3), 195–210.

Prein, A. F., Liu, C., Ikeda, K., Trier, S. B., Rasmussen, R. M., Holland, G. J., & Clark, M. P. (2017). Increased rainfall volume from future convective storms in the us. *Nature Climate Change*, *7*(12), 880–884.

Schaller, N., Kay, A. L., Lamb, R., Massey, N. R., Van Oldenborgh, G. J., Otto, F. E., ... others (2016). Human influence on climate in the 2014 southern england winter floods and their impacts. *Nature Climate Change*, *6*(6), 627–634.

Scoccimarro, E., & Gualdi, S. (2020). Heavy daily precipitation events in the CMIP6 worst-case scenario: Projected twenty-first-century changes. *Journal of Climate*, *33*(17), 7631–7642.

Shepherd, T. G. (2014). Atmospheric circulation as a source of uncertainty in climate change projections. *Nature Geoscience*, *7*(10), 703–708.

Sklar, M. (1959). Fonctions de repartition an dimensions et leurs marges. *Publ. inst. statist. univ. Paris*, *8*, 229–231.

Trzeciak, T. M., Knippertz, P., Pirret, J. S., & Williams, K. D. (2016). Can we trust climate models to realistically represent severe european windstorms? *Climate Dynamics*, *46*(11-12), 3431–3451.

van den Hurk, B., van Meijgaard, E., de Valk, P., van Heeringen, K.-J., & Gooijer, J. (2015). Analysis of a compounding surge and precipitation event in the netherlands. *Environmental Research Letters*, *10*(3), 035001. doi: 10.1088/1748-9326/10/3/035001

van der Wiel, K., Stoop, L. P., Van Zuijlen, B., Blackport, R., Van den Broek, M., & Selten, F. (2019). Meteorological conditions leading to extreme low variable renewable energy production and extreme high energy shortfall. *Renewable and Sustainable Energy Reviews*, *111*, 261–275.

Villalobos-Herrera, R., Bevacqua, E., Ribeiro, A. F., Auld, G., Crocetti, L., Mircheva, B., ... Michele, C. D. (2020). Towards a compound event-oriented climate model evaluation: A decomposition of the underlying biases in multivariate fire and heat stress hazards. *Natural Hazards and Earth System Sciences Discussions*. doi: https://doi.org/10.5194/nhess-2020-383

Wang, H., He, S., & Liu, J. (2013). Present and future relationship between the east asian winter monsoon and enso: Results of CMIP5. *Journal of Geophysical Research: Oceans*, *118*(10), 5222–5237.

Wang, L., & Chen, W. (2014). An intensity index for the east asian winter monsoon. *Journal of Climate*, *27*(6), 2361–2374.

Watson, P., Sparrow, S., Ingram, W., Wilson, S., Marie, D., Zappa, G., ... Allen, M. (2020). Multi-thousand member ensemble atmospheric simulations with global 60km resolution using climateprediction.net. In *Egu general assembly conference abstracts* (p. 10895). doi: https://doi.org/10.5194/egusphere-egu2020-10895

Williams, K., Ringer, M., & Senior, C. (2003). Evaluating the cloud response to climate change and current climate variability. *Climate Dynamics*, *20*(7-8), 705–721.

Zappa, G. (2019). Regional climate impacts of future changes in the mid–latitude atmospheric circulation: a storyline view. *Current Climate Change Reports*, *5*(4), 358–371.

Zappa, G., Hawcroft, M. K., Shaffrey, L., Black, E., & Brayshaw, D. J. (2015a). Extratropical cyclones and the projected decline of winter mediterranean precipitation in the CMIP5 models. *Climate Dynamics*, *45*(7-8), 1727–1738.

Zappa, G., Hoskins, B. J., & Shepherd, T. G. (2015b). The dependence of wintertime mediterranean precipitation on the atmospheric circulation response to climate change. *Environmental Research Letters*, *10*(10), 104012.

Zappa, G., Shaffrey, L. C., Hodges, K. I., Sansom, P. G., & Stephenson, D. B. (2013). A multimodel assessment of future projections of north atlantic and european extratropical cyclones in the CMIP5 climate models. *Journal of Climate*, *26*(16), 5846–5862.

Zappa, G., & Shepherd, T. G. (2017). Storylines of atmospheric circulation change for european regional climate impact assessment. *Journal of Climate*, *30*(16), 6561–6577.

Zscheischler, J., Martius, O., Westra, S., Bevacqua, E., Raymond, C., Horton, R., ... Vignotto, E. (2020). A typology of compound weather and climate events. *Nature Reviews Earth & Environment*, *1*, 333–347. doi: https://doi.org/10.1038/s41467-020-15665-3

Supporting Information for "Larger spatial footprint of wintertime total precipitation extremes in a warmer climate"

Emanuele Bevacqua[1], Theodore G. Shepherd[1], Peter A. G. Watson[2], Sarah Sparrow[3], David Wallom[3], and Dann Mitchell[2,4]

[1]Department of Meteorology, University of Reading, Reading, United Kingdom.

[2]School of Geographical Sciences, University of Bristol, Bristol, United Kigdom.

[3]Oxford e-Research Centre, Engineering Science, University of Oxford, Oxford, United Kingdom

[4]Cabot Insitute for the Environment, University of Bristol, Bristol, United Kingdom

Contents of this file

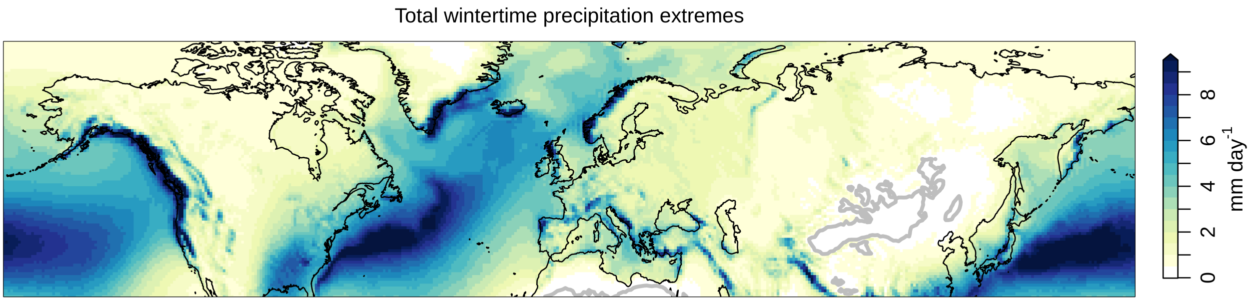

Figure S1. Local 10-year return level of the wintertime total precipitation based on HadAM4 model output for present-day climate. Grey contours over Asia enclose areas where the present-day 10-year return level is below 0.2mm/day (about 18mm/winter).

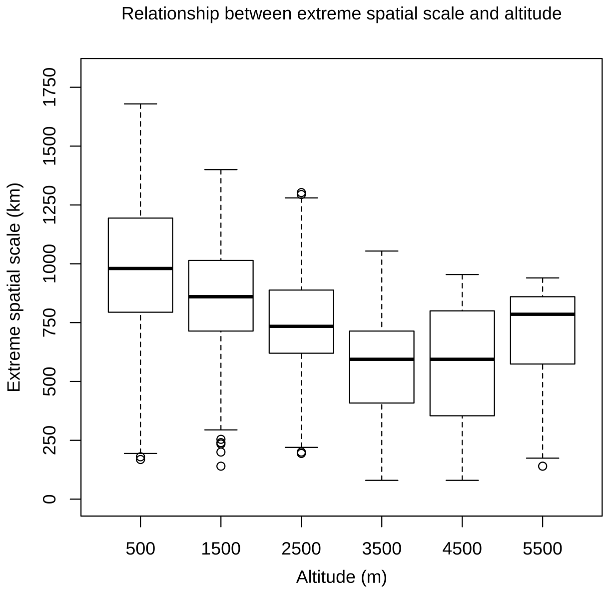

Figure S2. Boxplots showing the relationship between the grid-point local altitude and the present-day 100-year return level of the precipitation extremes' spatial scale (shown is the value of the radius associated with the spatial scale, as in Figure 1). Grid-points were binned based on their altitude by steps of 1000 meters above mean sea level, e.g., the bin labelled by 500m contains grid-points between 0 and 1000m.

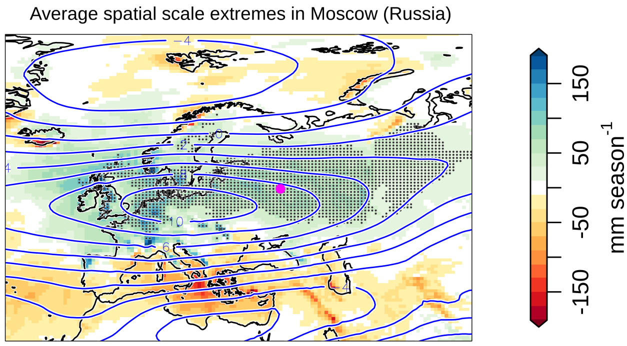

Figure S3. Average of the precipitation field anomaly associated with winters leading to extreme spatial scales (>100-year return level) around Moscow (Russia; shown with a magenta dot) in the present climate. Precipitation is shown with shading. Contours show the anomaly of the zonal wind at 250 hPa during the events (in m/s). Stippling indicates locations where the average precipitation value is higher than the local 10-year return level.

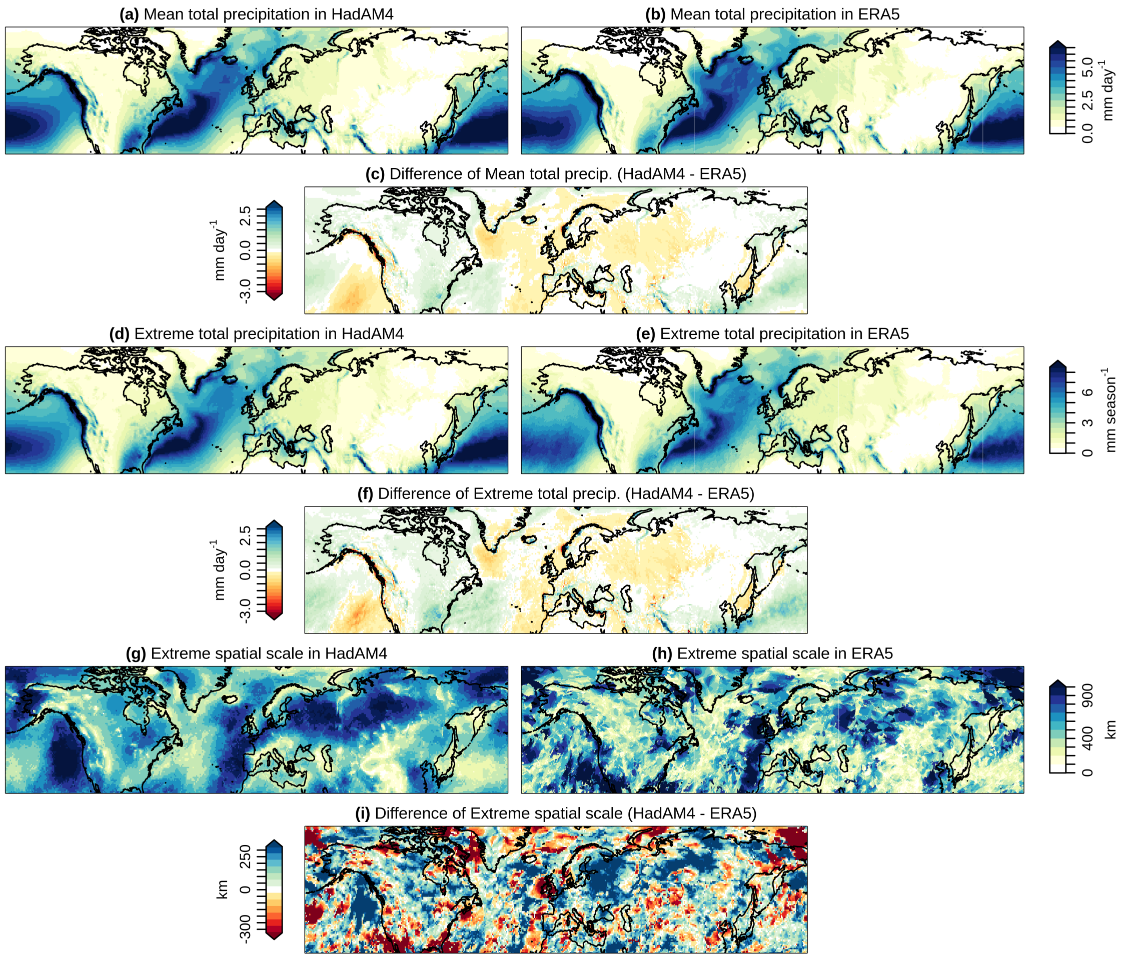

Figure S4. Comparison between precipitation statistics in the HadAM4 model (large ensemble of the period 2006-2015) and ERA5 reanalysis (1980-2020). Mean wintertime total precipitation based on (a) HadAM4 and (b) ERA5; panel (c) shows the difference between HadAM4 and ERA5 values. Extreme wintertime total precipitation (5-year return level) based on (d) HadAM4 and (e) ERA5; panel (f) shows their difference. Radius associated with the extreme spatial scale (computed based on $T_{\mathrm{occur}} = 5$ year and $T_{\mathrm{SS}} = 10$ year; see Methods) of wintertime total precipitation extremes based on (g) HadAM4 and (h) ERA5; panel (i) shows their difference. To compute the differences between HadAM4 and reanalysis, the ERA5 resulting fields are regridded to the native grid of HadAM4.

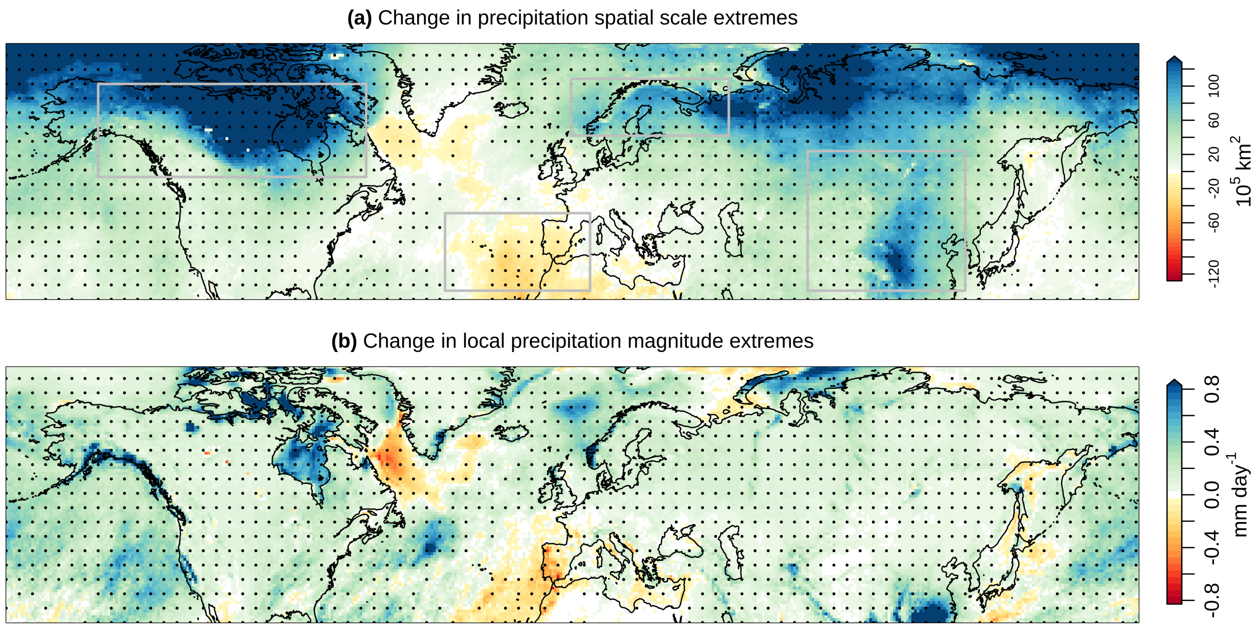

Figure S5. (a) As in Figure 2a, but showing the change in the spatial scale extremes in km^2 rather than the percentage change. Rectangles identify the regions referred to in the main text: (i) Canada, (ii) Northern Africa, Spain and Portugal, (iii) Northern Europe, and (iv) central and eastern Asia. (b) As in Figure 2d, but showing the change in mm.

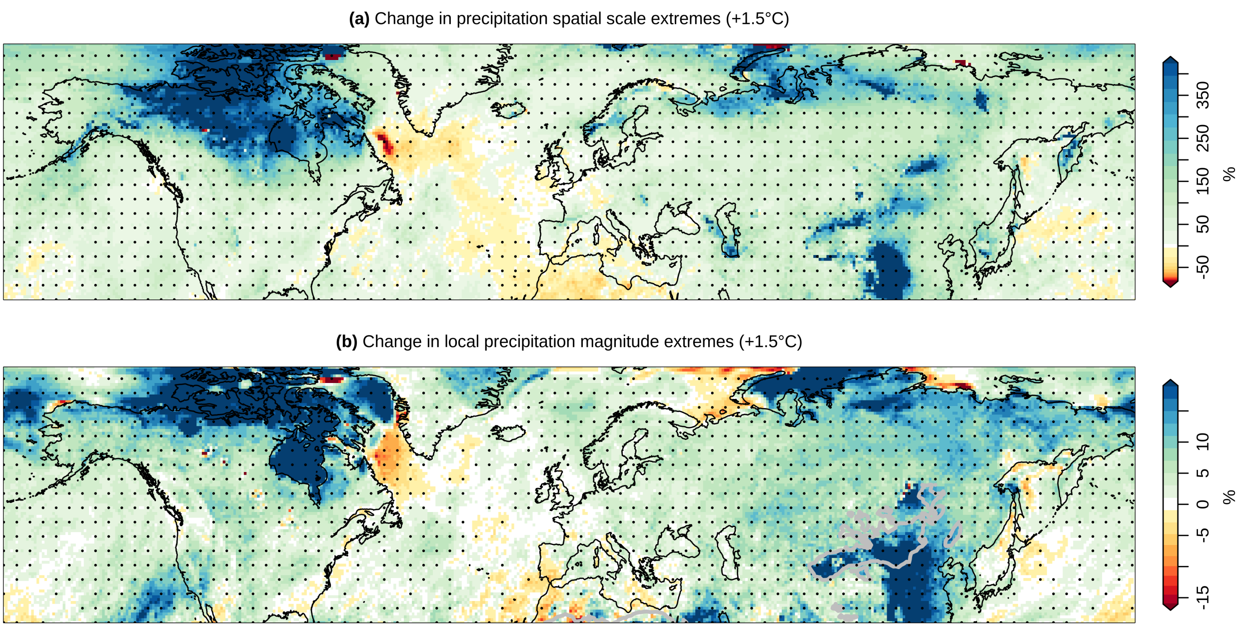

Figure S6. (a) As in Figure 2a, but under a 1.5^{o}C warming scenario. (b) As in Figure 2d, but under a 1.5^{o}C warming scenario.

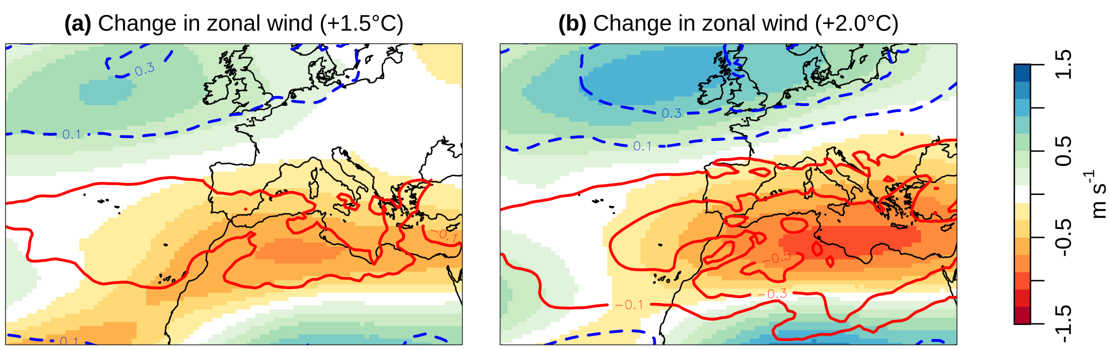

Figure S7. Changes in mean wintertime zonal wind at 250 hPa (shading) and 850 hPa (contours; in m/s) across Northern Africa and southern Europe under (a) 1.5^{o}C and (b) 2.0^{o}C warming scenario. Solid red indicates increase and dashed blue indicates a decrease in the wind at 850 hPa.

Table S1. Sensitivity of the changes, under a +2.0^{o}C warming, in the spatial scale extremes to variations in the return periods used to define extreme events.

		T_{SS} (years)		
		50	100	200
	5	93% (0%, 85%)	82% (0%, 74%)	78% (0%, 71%)
T_{occur} (years)	10	124% (0%, 120%)	97% (0%, 93%)	79% (0%, 78%)
	30	403% (0%, 385%)	201% (0%, 187%)	138% (0%, 126%)

Hemispheric *grid-point area-weighted median* of the changes (%) in spatial scale extremes for different combinations of return periods employed to define extreme events (i.e., T_{SS} and T_{occur}; defined in Methods). The two values (%) in the brackets are median changes driven by changes in the spatial dependencies and precipitation magnitudes, respectively. The table highlights that while the value of the median change depends on the considered return periods, the projected increase is a robust feature across different return periods. Changes driven by the precipitation spatial dependence are small for all considered return periods. Note that the spatial pattern of the changes in the spatial scale extremes is largely insensitive to variations in the return periods (not shown).

Table S2. As in Table S1, but showing the sensitivity of the ratio between the median change in the spatial scale extremes (based on T_{occur} and T_{SS}) and in the magnitude of wintertime total precipitation extremes (based on T_{occur}).

		T_{SS} (years)		
		50	100	200
	5	26	23	22
T_{occur} (years)	10	31	25	20
	30	94	47	32

Table S3. As in Table S1, but showing the sensitivity of the ratio between the median change in the spatial scale in a +2.0^{o}C and +1.5^{o}C warming scenario.

		T_{SS} (years)		
		50	100	200
	5	1.7	1.7	1.7
T_{occur} (years)	10	1.6	1.6	1.6
	30	2.0	1.8	1.8

Table S4. As in Table S1, but showing the sensitivity of the area fraction (%) exposed to an increase in the spatial scale extremes under a +2.0^{o}C warming scenario (results for +1.5^{o}C warming scenario are shown in brackets).

		T_{SS} (years)		
		50	100	200
	5	90% (91%)	90% (90%)	90% (89%)
T_{occur} (years)	10	90% (88%)	90% (87%)	89% (86%)
	30	87% (82%)	88% (83%)	87% (82%)

Table S5. As in Table S1, but showing the sensitivity of the present-day median spatial scale extremes and, in brackets, associated changes in a +2.0^{o}C warming scenario.

		T_{SS} (years)		
		50	100	200
	5	$67{\cdot}10^5 km^2$ ($63{\cdot}10^5 km^2$)	$90{\cdot}10^5 km^2$ ($74{\cdot}10^5 km^2$)	$110{\cdot}10^5 km^2$ ($87{\cdot}10^5 km^2$)
T_{occur} (years)	10	$15{\cdot}10^5 km^2$ ($22{\cdot}10^5 km^2$)	$27{\cdot}10^5 km^2$ ($29{\cdot}10^5 km^2$)	$39{\cdot}10^5 km^2$ ($33{\cdot}10^5 km^2$)
	30	$0.80{\cdot}10^5 km^2$ ($0.96{\cdot}10^5 km^2$)	$3.2{\cdot}10^5 km^2$ ($2.0{\cdot}10^5 km^2$)	$7.2{\cdot}10^5 km^2$ ($3.1{\cdot}10^5 km^2$)